APPLICATION OF FULL WAVEFORM ACOUSTIC LOGGING DATA TO THE ESTIMATION OF RESERVOIR PERMEABILITY

by

F. Mathieu and M.N. Toksöz

Earth Resources Laboratory
Department of Earth, Atmospheric and Planetary Sciences
Massachusetts Institute of Technology
Cambridge, MA. 02139

ABSTRACT

Development of borehole geophysics has recently focused on reservoir characterization. Within this effort, extensive full waveform acoustic surveys have demonstrated a correlation between the occurance of open fractures and attenuation of Stoneley waves. A relationship is obtained here between fracture permeability and attenuation of Stoneley waves, on the basis of a physical mechanism. This mechanism involves an energy transfer under the form of a fluid flow inside permeable formations. It is applied to the cases of a single open fracture, a multi-fractured medium and a homogeneous porous medium. Theoretical results show the effects of frequency, borehole radius, permeability, fracture density and porosity on attenuation. The single fracture theory is applied to observed attenuation data due to isolated large open fractures: the theoretical fracture apertures obtained compare favorably to values determined from packer tests.

NOMENCLATURE

A	attenuation of the Stoneley wave
A_A	amplitude attenuation
A_E	energy attenuation
b	diffusion equation coefficient
c	Stoneley wave phase velocity
d	fracture density
f	Stoneley wave horizontal wavenumber
h	width of a small layer in a porous medium
H	width of a fractured or porous medium
I_i	modified Bessel function of the i-th order
k	Stoneley wave vertical wavenumber
K	permeability
L	fracture width
L_a	fracture aperture obtained from inversion of the attenuation
L_p	fracture aperture obtained from packer tests
$P_D(r,t)$	fluid pressure distribution in the porous medium
$P_F(r,t)$	fluid pressure distribution in the fracture

P_I	incident Stoneley wave pressure in the borehole
P_R	transmitted Stoneley wave pressure in the borehole
P_T	reflected Stoneley wave pressure in the borehole
$q_D(r,t)$	rate of fluid flow in the porous medium
$q_F(r,t)$	rate of fluid flow in the fracture
q_I	rate of fluid flow in the borehole, associated with the incident Stoneley wave
q_R	rate of fluid flow in the borehole, associated with the reflected Stoneley wave
q_T	rate of fluid flow in the borehole, associated with the transmitted Stoneley wave
R	borehole radius
S_B	borehole cross-section
S_F	fracture cross-section
T	time period of the Stoneley wave
v_F	fluid particle velocity in the fracture
v_I	fluid particle velocity for the incident Stoneley wave
v_R	fluid particle velocity for the reflected Stoneley wave
v_T	fluid particle velocity for the transmitted Stoneley wave
v_{pf}	P-wave velocity in the fluid
Z_B	impedance of the borehole fluid flow
Z_F	impedance of the fracture fluid flow
α	attenuation coefficient in $P_T / P_I = exp(-\alpha z)$
γ	fluid compressibility
μ	dynamic fluid viscosity
ρ_f	fluid density
ω	Stoneley wave angular frequency
Θ_F	fracture impedance coefficient

INTRODUCTION

Borehole geophysics are being increasingly applied to reservoir characterization. In particular, full waveform acoustic logging surveys seem to be of great interest in identifying fractured zones in a reservoir. Such a technique could be very helpful in determining quantitatively the total permeability of a fractured hydrocarbon reservoir in carbonate formations, since it can be related to fracture permeability (Stearns and Friedman, 1969). In addition, applications can be found in other areas, such as mapping ground water flow for various purposes (Davison *etal*., 1982).

Field experiments with full waveform acoustic logging tools show a good correlation between fractures in crystalline formations and Stoneley wave attenuation in those formations. Iso-offset sections from ELF AQUITAINE's multi-offset tool E.V.A. show almost complete attenuation of P and S waves as well as partial attenuation of the Stoneley wave, opposite a portion of the formation where a hydro-fracturing experiment was conducted (Figure 1, Arens and Arditty, 1982). Similar attenuation of the whole wave train, including Stoneley waves, was correlated with the occurance of fractures by means of a televiewer log, on the Hi Vista well in Southern California, and a study (Moos and Zoback, 1983) focused on the P and S-wave velocities in such fractured crystalline rocks. Finally, an extensive survey in two well sites of Manitoba,

Canada, used full waveform logs, televiewer logs and hydrologic experiments to detect fractures in granite (Paillet, 1980; Davison *etal*., 1982). Figure 3 shows the correlation between fractures detected by a televiewer log and attenuation of the Stoneley wave at the corresponding depths.

In this paper, a model is derived which relates the fracture permeability and the attenuation of Stoneley waves. The proposed mechanism attributes the Stoneley wave attenuation to fluid flow inside the formation and reflection at the fracture interface. The mechanism is first analyzed for an isolated fracture and then extended to a homogeneously fractured medium. A variation of the theory is then used to model Stoneley wave attenuation in a porous medium. Subsequently, the effects of the model parameters on the computed attenuation are discussed. Finally, theoretical fracture permeabilities are obtained from real data and compared to values obtained from packer tests in wells.

THEORETICAL DEVELOPMENT

The proposed mechanism for the attenuation of Stoneley waves involves the transfer of part of the Stoneley wave energy to a fluid flow in the permeable formation. Consider an incident Stoneley wave propagating along a borehole. A monochromatic Stoneley wave induces in the borehole fluid a pressure variation (Cheng and Toksöz, 1981)

$$P(r,z,t) = B\, I_0(fr)\, e^{i(\omega t - kz)} \tag{1}$$

with

$$f^2 = k^2 \left(1 - \frac{c^2}{v_{pf}^2}\right) \tag{2}$$

where ω is the frequency, c the phase velocity of the Stoneley wave, $k = \omega / c$ the vertical wavenumber, v_{pf} the P-wave velocity in the fluid, f the horizontal wavenumber and B a constant.

All calculations can be carried out for such a monochromatic wave, without loss of generality. The z-dependence of the Stoneley wave is similar to that of a compressional plane wave traveling along the z-axis. The wave train has a succession of alternating compressions and dilatations. Each compression provokes a pressure buildup at the interface between borehole and formation. Therefore, when a compression phase encounters the permeable formation, be it a single isolated fracture, a series of fractures in a "fractured medium", or a porous medium, the pressure gradient at the interface forces the fluid to diffuse into the fracture (Figure 4). Hence, part of the Stoneley wave energy is lost, resulting in its attenuation. The effect of the Stoneley wave propagating within the formation can be neglected in the case of "hard" formations because most of the energy is in the fluid (Cheng *etal*., 1982).

Theory for isolated fractures

The simplest case of an isolated fracture intersecting a vertical borehole of radius R is considered first. The fracture is modeled by a plane horizontal fluid layer of width L surrounded by an impervious "hard" formation, such as compact limestone or granite (Figure 5a). L is small in comparison to the wavelength of the Stoneley wave and the fracture length is long enough to be considered as infinite within the theory. The fluid in the fracture and the borehole is in equilibrium under hydrostatic pressure before the Stoneley wave arrival.

When a compression phase of the Stoneley wave hits the fracture, fluid is forced into the fracture. It is assumed that the diffusion process inside the fracture is over before the start of the dilatation phase, so that a similar but reversed mechanism can occur at the next half-period $T/2$. A good approximate solution for the diffused pressure (Appendix A(i), Figure 6) is given by

$$P_F(r,t) \approx P_F \left[\frac{R}{r}\right]^{1/2} erfc\left[\frac{(r-R)}{(4bt)^{1/2}}\right] \tag{3}$$

where

$$erfc(x) \equiv 1 - \left(\frac{2}{\pi^{1/2}}\right) \int_0^x exp(-\rho^2)\, d\rho \tag{4}$$

and

$$\frac{1}{b} = \frac{12\gamma\mu}{L^2} \tag{5}$$

The attenuation is defined by

$$A \equiv 1 - \frac{P_T}{P_I} \tag{6}$$

where P_T and P_I are respectively the incident and transmitted Stoneley waves (Figure 7a). The attenuation can be expressed after setting the appropriate boundary conditions. The problem is analogous to that of a plane sound wave propagating in a duct, and attenuated by an absorptive strip (Young, 1953). The transmission coefficient calculated in Appendix B(i) is

$$\frac{P_T}{P_I} = \frac{1}{1+X} \tag{7}$$

where

$$X = \frac{\rho_f c f}{24\mu} \frac{I_0(fR)}{I_1(fR)} \left[\frac{1}{2R} + \frac{2}{\pi}\left(\frac{\omega}{b}\right)^{1/2}\right] L^3 \tag{8}$$

Application to the case of a homogeneously fractured medium

The fracture width L is an adequate parameter for the case of a single fracture. However the offsets of full waveform acoustic logging tools generally do not make it possible to isolate a single fracture and they integrate the effects of several fractures in the overall attenuation. Therefore, the permeability K is substituted for L as the parameter describing a fractured medium of thickness H, made of a density d of even and regularly spaced fractures (Figure 5b, Appendix A(ii)). The fracture pressure is still given by equation (3) but in terms of K and d. Its coefficient b is such that

$$\frac{1}{b} = \gamma\mu\left(\frac{12d^2}{K^2}\right)^{1/3} \tag{9}$$

For a single fracture, the transmission coefficient is still given by equation (7), and X given by

$$X = \frac{\rho_f c f}{2\mu}\frac{I_0(fR)}{I_1(fR)}\left(\frac{1}{2R} + \frac{2}{\pi}\left(\frac{\omega}{b}\right)^{1/2}\right)\frac{K}{d} \tag{10}$$

For the total layer of thickness H, $n = Hd$ is the number of fractures in this layer. The effect of the upgoing reflected waves on the boundary conditions can be neglected in comparison to the downgoing incident wave, since the reflection coefficient of a single fracture is much smaller than 1. The transmission coefficient of the layer is

$$\left(\frac{P_T}{P_I}\right)_H = \left(\frac{P_T}{P_I}\right)^n \tag{11}$$

As $X \ll 1$ for large densities, equation (11) can be approximated by

$$\left(\frac{P_T}{P_I}\right)_H \approx e^{-nX} \tag{12}$$

Theory for a porous medium

It is reasonable to assume that Stoneley waves can be attenuated along any kind of porous medium. In such a general porous medium, the flow properties are governing its permeability K and its porosity φ. Darcy's law and the continuity equation, respectively, take both into account. In the case of fractures, these equations are connected by a relation between K and the width L of a single fracture, in other words by means of an implicit porosity model, in which all the fluid is contained within parallel planes. Here, the porosity is an external parameter, in the same sense as the fracture density discussed in the previous section, and is the interconnected porosity.

The diffused pressure in the porous medium (Appendix A(iii), figure 7b) is given by equation (3), changing the subscript F for "fracture" into the subscript D for "diffused", and b is such that

$$\frac{1}{b} = \frac{\varphi \gamma \mu}{K} \tag{13}$$

Figure 7b and Appendix B(ii) show the new boundary conditions. The attenuation is still defined by equation (6). The transmission coefficient for a thin layer of thickness h is

$$\frac{P_T}{P_I} = \frac{1}{1 + X} \tag{14}$$

with

$$X = \alpha h \tag{15}$$

where

$$\alpha = \frac{\rho_f c f}{\mu} \frac{I_0(fR)}{I_1(fR)} \left(\frac{1}{2R} + \frac{2}{\pi} \left(\frac{\omega}{b} \right)^{1/2} \right) K \tag{16}$$

and b is given by equation (13).

Application to the case of an extended porous medium

When the thickness H of the porous medium is of the same order of magnitude or larger than the wavelength, it is no longer possible to apply the boundary conditions of Appendix B(ii) directly. However, for a thin layer of width h within the medium (Figure 7b), much thicker than the pore dimensions but thin enough for the coefficient X in equation (16) to verify $X \ll 1$, the transmission coefficient for that layer can be approximated by

$$\left(\frac{P_T}{P_I} \right)_h \approx e^{-\alpha h} \tag{17}$$

where α is given by equation (16). Therefore, the total transmission coefficient for the porous medium of thickness H is

$$\left(\frac{P_T}{P_I} \right)_H \approx e^{-\alpha H} \tag{18}$$

RESULTS AND DISCUSSION

The theoretical attenuations just derived depend on three subsets of parameters: formation and fluid parameters, frequency and borehole radius, and flow parameters of the medium (permeability and porosity).

Formation parameters only appear through the period equation of the Stoneley wave. They have little effect on the attenuation, as the Stoneley wave is only slightly dispersive. Fluid parameters do not change as much as formation parameters. Therefore, only the second and third subsets of parameters are likely to have a major effect on attenuation.

The results presented in this section are divided into three parts. First, the frequency and borehole radius effects on attenuation are shown. Second, the effects of permeability and porosity are evaluated and the possibility that the two parameters are correlated is discussed. Finally, some permeabilities (fracture widths) obtained from packer tests on isolated fractures are compared with permeabilities determined from full waveform data, using the present theory.

The effect of frequency and borehole radius variations on attenuation.

The usual frequencies of full waveform acoustic logging tools range between 1 and 40 Khz. For example, peak frequency of Stoneley waves recorded by ELF AQUITAINE's tool E.V.A. is about 6 kHz, while that of the U.S.G.S. tool is 34 kHz. Figures 8-10 show that attenuation increases slightly with increasing frequency. This is valid for isolated fractures of different widths (Figure 9) as well as for porous media of different permeabilities (Figure 10). Such low dispersion implies that attenuation will be very similar over a narrow enough frequency spectrum. Therefore, the best way to invert attenuation of a real signal for permeability is to calculate the theoretical attenuation for the central frequency of the Stoneley wave.

Variation in the borehole radius R affects attenuation in a much more drastic way. The phase velocity is only slightly affected by a change of R. However, the coefficients $I_0(fR)/I_1(fR)$ and $1/2R$ in equations (8), (10) and (16) control the R dependence of attenuation. The predominant factor is $1/2R$. Figure 11 shows that in boreholes with smaller radii the observed attenuation are greater.

The effect of permeability and porosity variations on attenuation.

Figures 12 and 13 show how the attenuations in the thinly fractured medium and the porous medium approaches depend on fracture density and porosity, respectively. A greater porosity and a greater permeability produce a greater attenuation (Figure 13). This result supports intuition and agrees with the observations of Staal and Robinson (1977) and with the results of Rosenbaum's theory (Rosenbaum, 1974). It may not be obvious intuitively, however, that, for a given permeability, many fractures of a lesser width produce more attenuation than fewer fractures of a greater width (Figure 12).

However, this is evident from equation (12), where $nX=hdX$ only involves $d^{1/3}$ in the coefficient $2/\pi(\omega/b)^{1/2}$.

In the case of a fractured zone, the dependency between porosity and permeability is implicit in the model of parallel plates (Figure 5b). As porosity is defined as an external parameter in the porous medium theory, an "a-priori" dependence on permeability is not assumed. However, the two parameters are generally dependent. The curves of Figure 13 are calculated without introducing porosity-permeability dependence.

It would be gratifying to link the two approaches in a model applicable to both. The parallel plates model, as a specific porous medium, may be such a model. However, the boundary conditions are different in that reflected waves are only considered in the fractured medium model, a porous medium being too smooth to generate them. Therefore, no comparison can be made between the two approaches, and they should be tested separately on real data. According to the lithology porous sandstones are likely to adapt well to the porous medium theory, whereas fractured carbonates or crystalline rocks will be better handled with the single fracture or the fracture density theory.

Determination of fracture apertures from observed attenuation data and comparison with packer test results.

Figure 3 showed good correlation between Stoneley wave attenuation and open fractures, as evidenced by a televiewer log. This subset of data belongs to a fairly exhaustive survey made in Canada for the purpose of nuclear waste storage in granite (Paillet, 1980; Davison *etal.*, 1982). Hydrologic tests were used in addition to borehole geophysics logs. Some packer tests designed to straddle single, open fractures evidenced by cores and televiewer logs, are available jointly with Stoneley wave attenuation values on the same fractures.

The Stoneley wave energy attenuation A_E (Paillet, 1980) is first transformed into an amplitude attenuation A_A by means of

$$A_A = 1 - [1-A_E]^{1/2} \tag{19}$$

Fracture widths are then obtained from an attenuation versus fracture width plot (Figure 14). Physical parameters required to model the attenuation from equation (8) are listed in Table 1. Spectral analysis (Paillet, 1980) yielded a central frequency of 34 Khz for the Stoneley wave. Attenuation is computed here on the basis of this value.

Similarly, fracture apertures were estimated from fluid-injection tests, using a single fracture model (Davison *etal.*, 1982). Results of the comparison between the two estimates are listed in Table 2, including the relative deviation $\Delta L/L_p$ of the acoustic estimate L_a versus the packer test estimate L_p.

Obviously, some limiting factors have to be considered before interpreting the results. First, the depth of penetration of the flows are very dissimilar (10 to 100 meters in the case of fluid-injection tests, much less than 1 meter in the

case of a diffused wave). Second, the nature of the flow is different (steady injection in the first case, high frequency steady-state flow in the second case), and permeabilities are unlikely to be the same for such different flow conditions.

In the theoretical developments, three simplifications were made: 1) there are no obstructions in the fractures to laminar flow (i.e., no turbulence, irregular walls or loose particles); 2) the "return flow" from formation into the borehole is small and does not contribute to the energy of the Stoneley waves; and 3) there is no diffraction (scattering) of acoustic energy into other wave modes. The first condition biases the theoretical results towards lower fracture densities for given permeabilities. However, it does not affect the overall permeability value for a given observed attenuation. The second condition implies that we assume the maximum attenuation for a given permeability. Thus theoretical permeability calculated from attenuation may be lower than the actual value. The third assumption means that we ignore attenuation due to elastic scattering (as shown in Fig. 1) and attribute all attenuation to permeability. thus we introduce a bias towards greater permeability.

Given these limitations the comparisons between the packer test results and computed permeability based on our theory are extremely good except for case 5 at depth 424 m and case 6 at depth 468 m (Table 2). These two discrepancies are most likely due to possible changes in fracture properties away from the borehole.

On the whole, however, Table 2 shows very good agreement between both approaches for obtaining in-situ permeability due to large fractures. The packer test might be more flexible for determining the permeability due to extended fractures, because of its larger and variable depth of penetration. On the other hand, a borehole survey gives fast and very early results in the history of a well, and is relatively inexpensive. Therefore, permeability detection from acoustic surveys could add much value to the full waveform acoustic logging method.

More work is necessary to improve and test the present theory. The effect of dipping fractures with respect to the borehole is currently being investigated. However, fractures intersecting at high angles (greater than 70^0) introduce additional complication and therefore can't be considered within the theory (Paillet, 1980). Additional measurables such as attenuation of P waves could add additional constraints to permeability determination. Finally, the diffraction mechanism could be dealt with in a finite element scheme, taking into account Stoneley waves in the formation as well as in the borehole fluid. This approach might yield better results for thin fractures.

CONCLUSION

Good correlation between the occurance of open fractures in crystalline formations and the attenuation of Stoneley waves led to the belief that a physical mechanism could attenuate the amplitude of the Stoneley wave. The core of the theory involves an irreversible energy transfer from the Stoneley wave into the fracture fluid. Research aimed at building a theory on the basis of

this mechanism was motivated by its potential application to permeability detection in a fractured reservoir. In the process of designing a theory that could account for the attenuation of the Stoneley wave amplitude in fractured media, another theory was set up to describe a similar process in the case of a porous medium.

An extensive borehole survey in Canadian crystalline fractured formations (Davison *etal.*, 1982) provided a basis to test the single fracture theory. From real attenuation data, theoretical apertures of large open fractures were obtained, with all other parameters fixed by the survey conditions. Those values compare very favorably to apertures deduced from packer tests designed to straddle the same fractures. The theory could therefore be of great help in giving an estimate of permeability in fractured reservoirs, or checking the effectiveness of hydrofracturing experiments, rapidly and at a low cost.

ACKNOWLEDGEMENTS

This research was supported by the company ELF AQUITAINE and the Full Waveform Acoustic Logging Consortium of the Earth Resources Laboratory at M.I.T. We are very much indebted to W.B. Beydoun of E.R.L. for the many valuable discussions throughout this research. We also thank F. Paillet of the U.S.G.S. for the initial idea and the access to the data. D. Dubucq and T. Keho were very helpful in reviewing the theoretical development. F. Mathieu is an ELF AQUITAINE fellow at M.I.T.

Table 1.

Physical parameters used to invert attenuation for fracture aperture.
Full waveform acoustic survey in granite (Paillet, 1980)

	$v_p(m/s)$	$v_s(m/s)$	$\rho(kg/m^3)$
granite	5850	3350	2650
fluid	1500	0	1000
fluid viscosity	μ	$= 10^{-3}$	Poiseuilles
fluid incompressibility	γ^{-1}	$= 2.\ 10^{9}$	Pa
borehole radius	R	= 0.038	m

Table 2.

Fracture apertures comparison for the full waveform acoustic and packer test approaches.					
Depth(m)	A_E	A_A	$L_a(\mu m)$	$L_p(\mu m)$	$\Delta L / L_p$ (%)
1) 450. (WN1)	0.44	0.25	173.	197.	-12.
2) 417. (WN1)	0.47	0.27	183.	265.	-31.
3) 430. (WN1)	0.50	0.29	187.	126.	+48.
4) 442. (WN1)	0.62	0.38	220.	186.	+17.
5) 424. (WN1)	0.28	0.15	133.	18.	+639.
6) 468. (WN4)	0.32	0.18	150.	46.	+226.
L_a: Acoustic value			L_p: Packer test value		

APPENDIX A

Radial flow in the formation

(i) Fluid layer approach

Consider an isolated fracture modeled by a plane fluid layer perpendicular to the borehole (figure 5a). Under the assumption of a one-dimensional laminar flow, Darcy's law relates the fluid flow rate diffused inside the fracture $q_F(r,t)$ to the pressure gradient $\partial P_F(r,t)/\partial r$ as

$$q_F(r,t) = -\frac{K L}{\mu} 2\pi r \frac{\partial P_F(r,t)}{\partial r} \tag{A.1}$$

where K is the fracture permeability, μ the fluid viscosity and L the fracture width. Assuming the fracture walls are rigid (i.e. L is a constant), the continuity equation relates $\partial q_F(r,t)/\partial r$ to $\partial P_F(r,t)/\partial t$ as

$$\frac{\partial q_F(r,t)}{\partial r} = -2\pi r L \gamma \frac{\partial P_F(r,t)}{\partial t} \tag{A.2}$$

where γ is the compressibility of the fluid (Beydoun *etal*.,1983). Rigorously, Darcy's law should only be applied to a porous medium. Equation (A.1) should therefore be modified, using the identity (Van Golf-Racht, 1982)

$$K = \frac{L^2}{12} \tag{A.3}$$

characteristic of a fluid layer. Combining (A.1), (A.2) and (A.3) yields the diffusion equation

$$\frac{1}{r}\frac{\partial}{\partial r}\left[r\frac{\partial P_F(r,t)}{\partial r}\right] = \frac{1}{b}\frac{\partial P_F(r,t)}{\partial t} \tag{A.4}$$

where

$$\frac{1}{b} = \frac{12\gamma\mu}{L^2} \tag{A.5}$$

A compression phase of the Stoneley wave is defined as one positive half cycle of a sine wave. Figure 6 shows how this pressure function imposed at the fracture boundary is approximated by a boxcar function. A simple finite difference analysis shows that attenuations computed with this approximation are very close (less than 5% error) to what the actual sine dependency would have given. The solution of (A.4) near the borehole for such a boundary condition is (Rice and Cleary, 1976)

$$P_F(r,t) \approx P_F\left[\frac{R}{r}\right]^{1/2} erfc\left[\frac{(r-R)}{(4bt)^{1/2}}\right] \tag{A.6}$$

where

$$erfc(x) \equiv 1 - \left(\frac{2}{\pi^{1/2}}\right)\int_0^x exp(-\rho^2)\,d\rho \tag{A.7}$$

The flow $q_F(R,t)$ inside the fracture is obtained from Darcy's law (A.1). After some algebra,

$$q_F(R,t) = \frac{L^3}{6\mu}\pi R P_F\left[\frac{1}{2R} + \frac{1}{(\pi bt)^{1/2}}\right] \tag{A.8}$$

(ii) Fracture density approach

In the case of a medium of fracture density d, the permeability K of the medium, the width L of a single fracture and d are related by

$$K = \frac{dL^3}{12} \tag{A.9}$$

Equation (A.1) is changed in

$$q_F(r,t) = -\frac{K}{\mu d}2\pi r\frac{\partial P_F(r,t)}{\partial r} \tag{A.10}$$

Equation (A.2) is still valid and its combination with (A.9) and (A.10) yields the diffusion equation (A.4) where

$$\frac{1}{b} = \gamma\mu \frac{Ld}{K} = \gamma\mu\left[\frac{12d^2}{K^2}\right]^{1/3} \tag{A.11}$$

(iii) Porous medium approach

Considering a porous layer of thickness h, permeability K and porosity φ (Figure 7b), under the assumption of a radial laminar flow, Darcy's law relates the diffused flow rate $q_D(r,t)$ to the pressure gradient $\partial P_D(r,t)/\partial r$ as

$$q_D(r,t) = -\frac{K h}{\mu} 2\pi r \frac{\partial P_D(r,t)}{\partial r} \tag{A.12}$$

The continuity equation relates $\partial q_D(r,t)/\partial r$ to $\partial P_D(r,t)/\partial t$ as

$$\frac{\partial q_D(r,t)}{\partial r} = -2\pi r h \varphi \gamma \frac{\partial P_D(r,t)}{\partial t} \tag{A.13}$$

Combining equations (A.11) and (A.12) yields the diffusion equation for a porous layer

$$\frac{1}{r}\frac{\partial}{\partial r}\left[r\frac{\partial P_D(r,t)}{\partial r}\right] = \frac{1}{b}\frac{\partial P_D(r,t)}{\partial t} \tag{A.14}$$

where

$$\frac{1}{b} = \frac{\varphi \gamma \mu}{K} \tag{A.15}$$

APPENDIX B

Boundary conditions

(i) Fluid layer approach

Due to the discontinuities at the edges of the fracture, the incident pressure wave P_I (Figure 6a) is assumed to be scattered in the form of a reflected wave P_R and a transmitted wave P_T. Since the fracture width L is small compared to the wavelength of the Stoneley wave, the reflected and transmitted waves can be considered as Stoneley waves of phase velocity c.

Pressure continuity can be written

$$P_I + P_R = P_T \tag{B.1}$$

$$P_T(R) = P_F(R) \tag{B.2}$$

where $P_T(R)$ and $P_F(R)$ are the transmitted pressure and the fracture pressure at the borehole-fracture boundary (r=R).

Volume conservation relates the incident fluid flow across the borehole cross-section q_I, the transmitted flow q_T and the diffused flow into the fracture $q_F(R)$

$$q_I = q_T + q_F(R) \tag{B.3}$$

All quantities are averaged over a half period of time $T/2$ corresponding to a compressive phase of the Stoneley wave. The three equations (B.1), (B.2) and (B.3) provide a unique solution for the unknowns P_R/P_I, P_T/P_I and P_F/P_I. There only remains to connect equations (B.1), (B.2) and (B.3). To do so, the concept of normal acoustic impedance is introduced:

$$Z = \frac{< P >}{< v >} \tag{B.4}$$

where $< P >$ and $< v >$ are respectively the averages of pressure and particle velocity over the flow cross-section. Applying this concept, equation (B.3) can be written

$$S_B v_I = S_B v_T + S_F v_F \tag{B.5}$$

in which

$$v_I = \frac{1}{Z_B}(P_I - P_R) \quad v_T = \frac{P_T}{Z_B} \quad v_F = \frac{P_F}{Z_F} \tag{B.6}$$

where Z_B and Z_F are respectively the borehole and fracture impedances, S_B and S_F the borehole and fracture cross-sections, velocities and pressures being averaged over those cross-sections.

The transmission coefficient comes from equations (B.1), (B.2), (B.5) and (B.6)

$$\frac{P_T}{P_I} = \frac{1}{1 + X} \tag{B.7}$$

with

$$X = \frac{fL}{2} \frac{I_0(fR)}{I_1(fR)} \frac{Z_B}{Z_F} \tag{B.8}$$

Impedances are calculated from (B.4). The borehole impedance is

$$Z_B = \rho_f \, c \tag{B.9}$$

The fracture impedance depends on a factor Θ_F to be calculated for the different expressions of the fracture flow:

$$Z_F = \rho_f \, c \, \Theta_F \tag{B.10}$$

Ultimately, combining (B.8), (B.9) and (B.10),

$$X = \frac{fL}{2} \frac{I_0(fR)}{I_1(fR)} \frac{1}{\Theta_F} \tag{B.11}$$

The average over a half-period $T/2$ of the fluid flow inside a single fracture is

$$q_F(R) = \frac{L^3}{6\mu} \pi R P_F \left(\frac{1}{2R} + \frac{2}{\pi} \left(\frac{\omega}{b} \right)^{1/2} \right) \tag{B.12}$$

where L is the fracture width and b is given by (A.5). The coefficient Θ_F of the fracture impedance is such that

$$\frac{1}{\Theta_F} = \frac{\rho_f c}{24\mu} L^2 \left(\frac{1}{2R} + \frac{2}{\pi} \left(\frac{\omega}{b} \right)^{1/2} \right) \tag{B.13}$$

When the permeability K is the parameter, as in the case of a fracture density, the coefficient Θ_F of the fracture impedance is such that

$$\frac{1}{\Theta_F} = \frac{\rho_f c}{\mu} \frac{K}{Ld} \left(\frac{1}{2R} + \frac{2}{\pi} \left(\frac{\omega}{b} \right)^{1/2} \right) \tag{B.14}$$

where L is the fracture width and b is given by (A.11).

(ii) Porous medium approach

For a layer of porous medium of width h (Figure 7b), it is reasonable to assume the absence of a reflected wave, as pores in a porous medium such as porous sandstone are smaller scale inhomogeneities than fractures in a fractured medium. The width h is still considered to be small compared to the wavelength of the Stoneley wave of phase velocity c. Thank's again to this property, it is assumed that

$$P_T(R) = P_D(R) \tag{B.15}$$

where $P_T(R)$ and $P_D(R)$ are the transmitted pressure and the diffused pressure

at the borehole-fracture boundary (r=R). Volume conservation relates the incident fluid flow q_I, the transmitted flow q_T and the diffused flow into the porous medium $q_D(R)$

$$q_I = q_T + q_D(R) \tag{B.16}$$

Following the same development as in (i), the transmission coefficient is

$$\frac{P_T}{P_I} = \frac{1}{1+X} \tag{B.17}$$

with

$$X = \alpha h \tag{B.18}$$

where

$$\alpha = \frac{\rho_f c f}{\mu} K \frac{I_0(fR)}{I_1(fR)} \left[\frac{1}{2R} + \frac{2}{\pi} \left[\frac{\omega}{b} \right]^{\frac{1}{2}} \right] \tag{B.19}$$

and b is given by equation (A.15).

REFERENCES

Arens, G., Arditty, P., 1982, Traitement et interprétation des diagraphies acoustiques EVA; Rapport Interne S.N.E.A.(P.).

Beydoun, W.B., Cheng, C.H. and Toksöz, M.N., 1983, Detection of subsurface fractures and permeable zones by the analysis of tube waves: Annual report 1983, Full waveform acoustic consortium, Earth Resources Laboratory, Department of Earth and Planetary Sciences, M.I.T.

Cheng, C.H. and Toksöz, M.N., 1981, Elastic wave propagation in a fluid-filled borehole and synthetic acoustic logs: *Geophysics*, v.46,p.1042-1053.

Cheng, C.H., Toksöz, M.N. and Willis, M.E., 1982, Determination of in situ attenuation from full waveform acoustic logs: *Jour. Geoph. Res.*, v.87,p.5477-5484.

Davison, C.C., Keys, W.S., Paillet, F.L., 1982, Use of borehole-geophysical logs and hydrologic tests to characterize crystalline rock for nuclear-waste storage, Whiteshell Nuclear Research Establishment, Manitoba, and Chalk River nuclear Laboratory, Ontario, Canada; Technical report, ONWI-418.

Moos, D. and Zoback, M.D., 1983, In situ studies of velocity in fractured crystalline rocks, *Jour. Geoph. Res.*, v.88, p.2345-2358.

Paillet, F.L., 1980, Acoustic propagation in the vicinity of fractures which intersect a fluid-filled borehole: S.P.W.L.A., 21 Symp., DD.

Rice, J.R. and Cleary, M.P., 1976, Some basic stress diffusion solutions for fluid-saturated elastic porous media with compressible constituents: *Rev. Geoph. Space Phys.*, v.14,No.2, p.227-241.

Rosenbaum, J.H., 1974, Synthetic microseismograms: Logging in porous formations; *Geophysics*, v.39,p.14-32.

Staal, J.J., and Robinson, J.D., 1977, Permeability profiles from acoustic logging: S.P.E. paper no. 6821 presented at the 52nd Ann. Fall Tech. Conf. and Exh. of the Soc. of Pet. Eng. of AIME, Denver, CO.

Stearns, D.W. and Friedman, M., 1969, Reservoirs in fractured rock, Am. Assoc. Petroleum Geologists, Memoirs 16,p.82-106.

Van Golf-Racht, T.D., 1982, *Fundamentals of fractured reservoir engineering;* Elsevier.

Young, J.E., 1953, Propagation of sound in attenuating ducts containing absorptive strips, Ph-D Thesis; M.I.T.

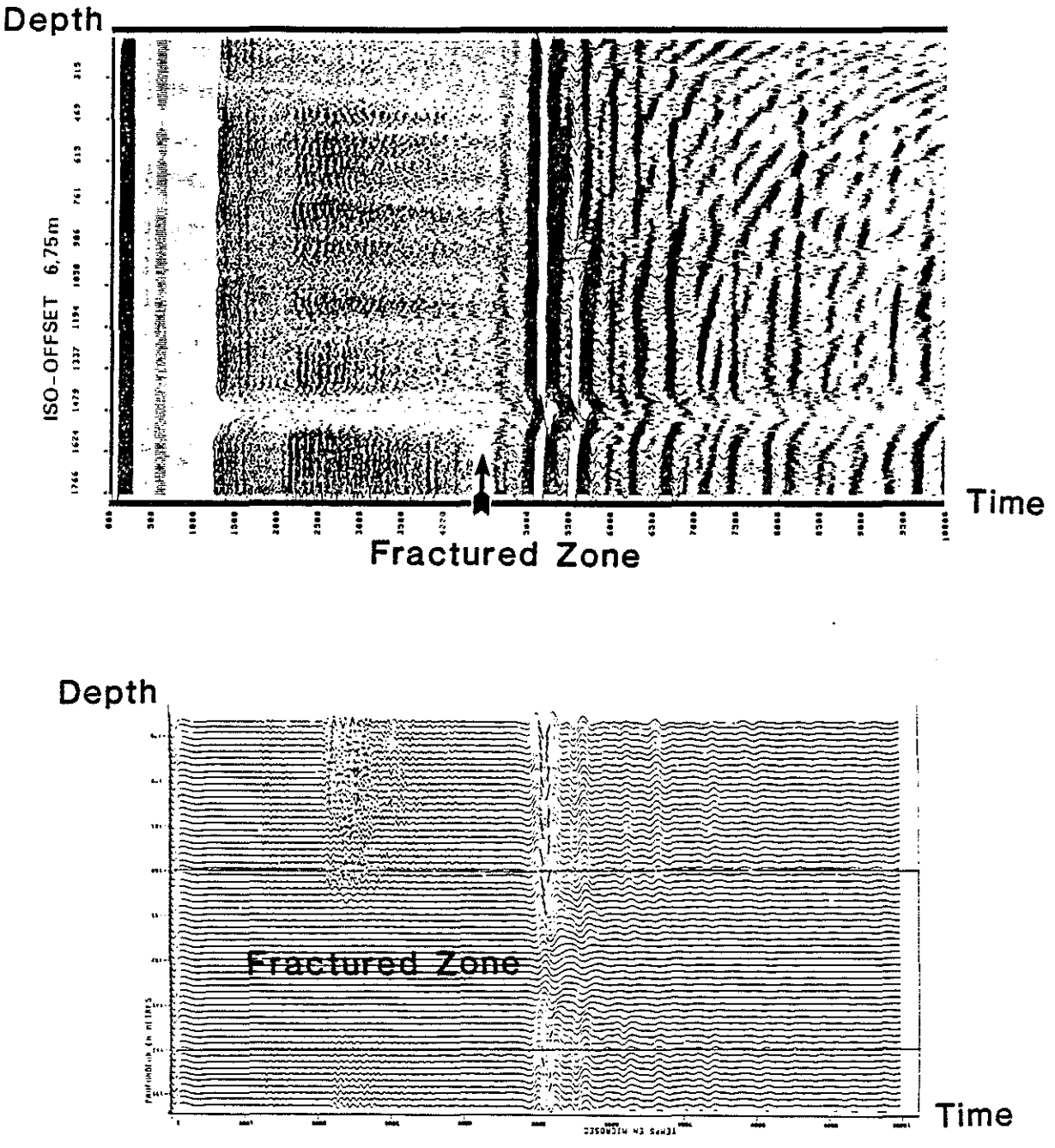

Figure 1: Full waveform acoustic data recorded after a hydrofracturing experiment (E.V.A.-Elf Aquitaine, 1982).

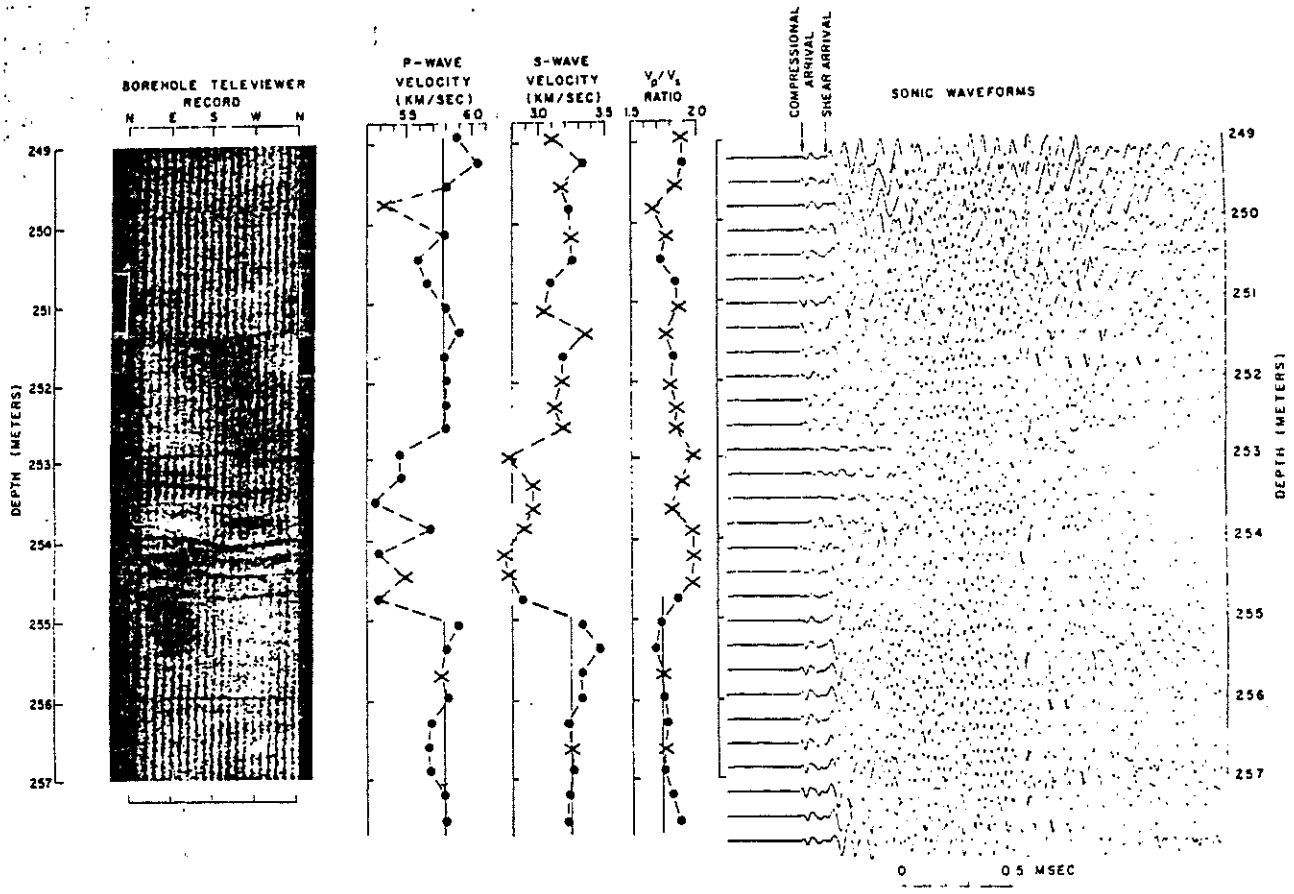

Figure 2: Correlation between fractures detected by a borehole televiewer and the attenuation of the complete acoustic wave train (Moos and Zoback, 1983).

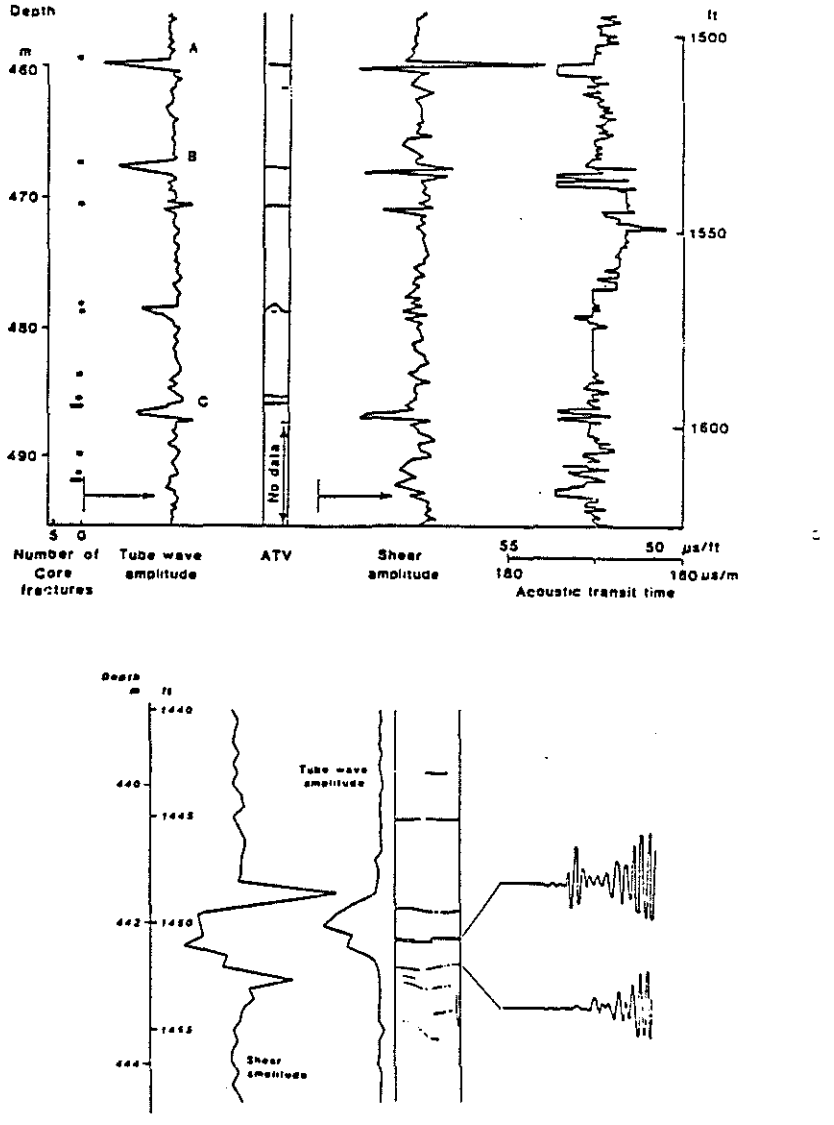

Figure 3: Correlation between fractures detected by a borehole televiewer (ATV) and the attenuation of the Stoneley wave (tube wave) (Paillet, 1980).

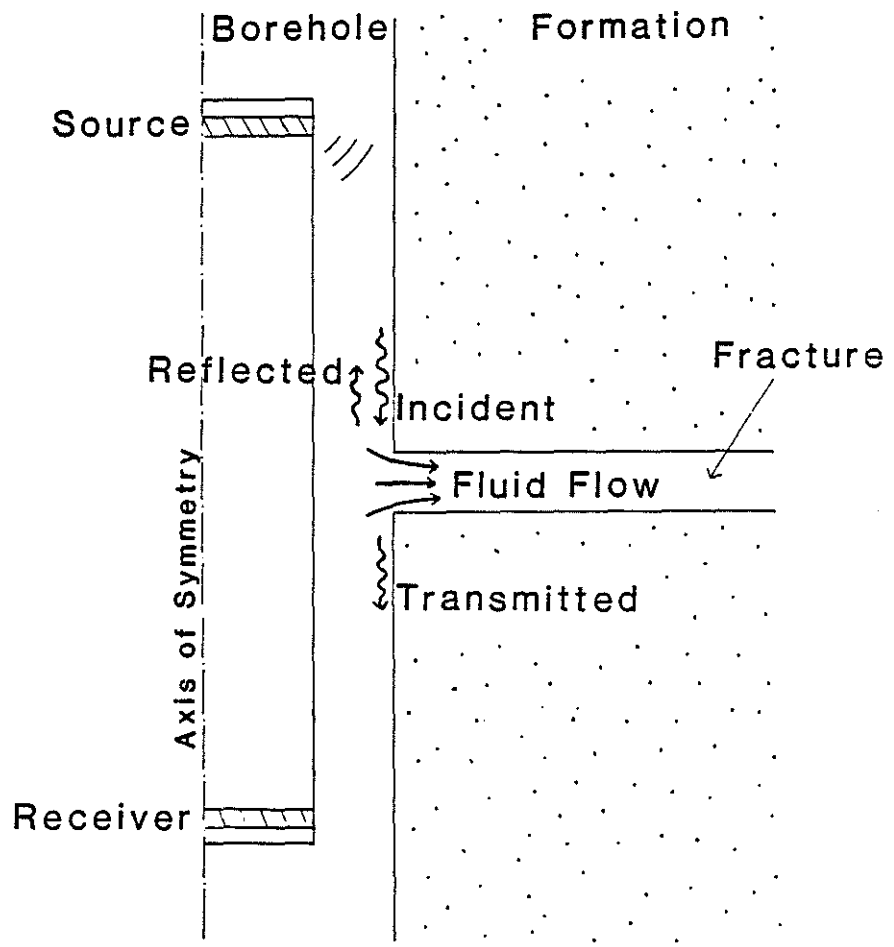

Figure 4: The attenuation mechanism in the case of a single fracture.

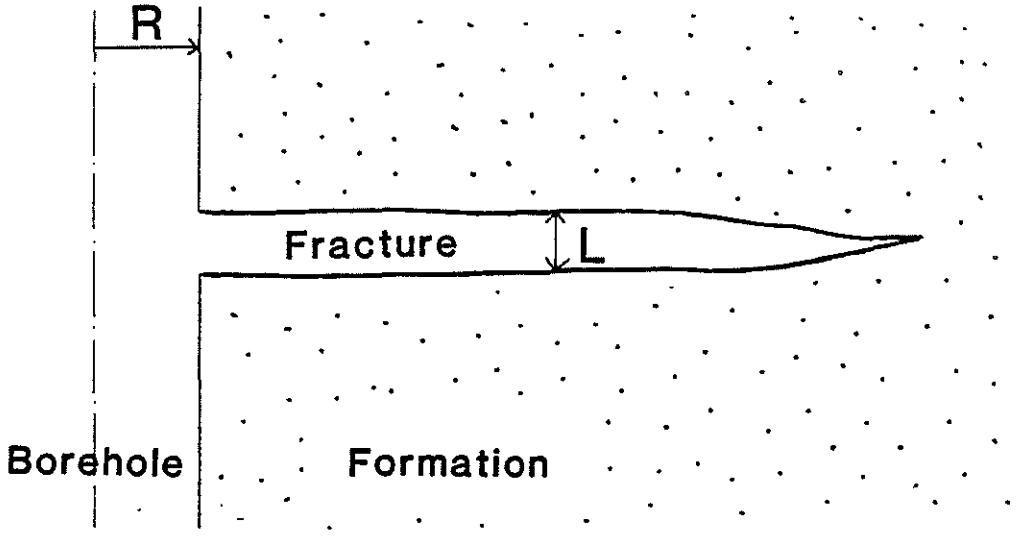

Figure 5a: Single fracture model.

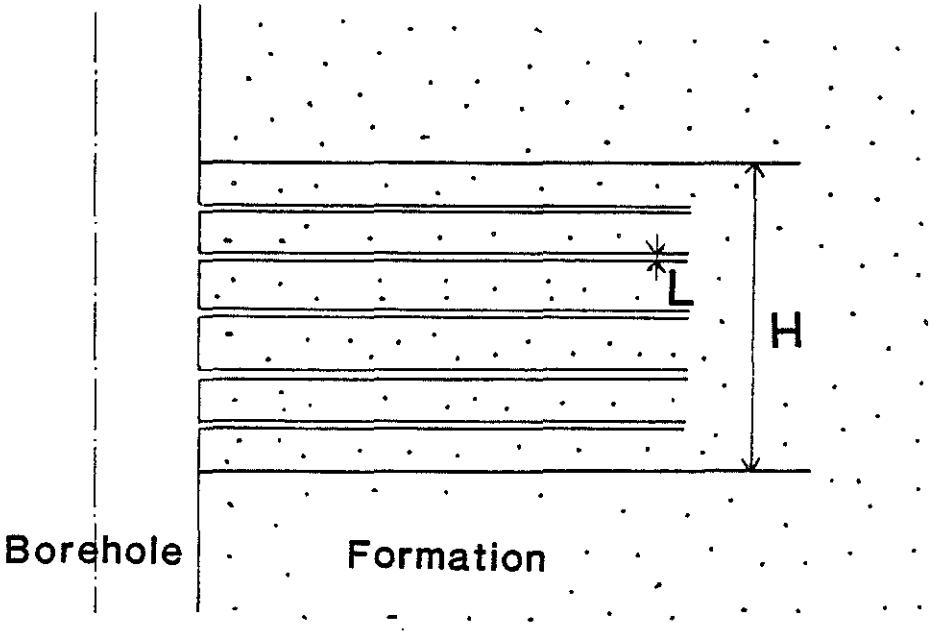

Figure 5b: Model for a multi-fractured medium.

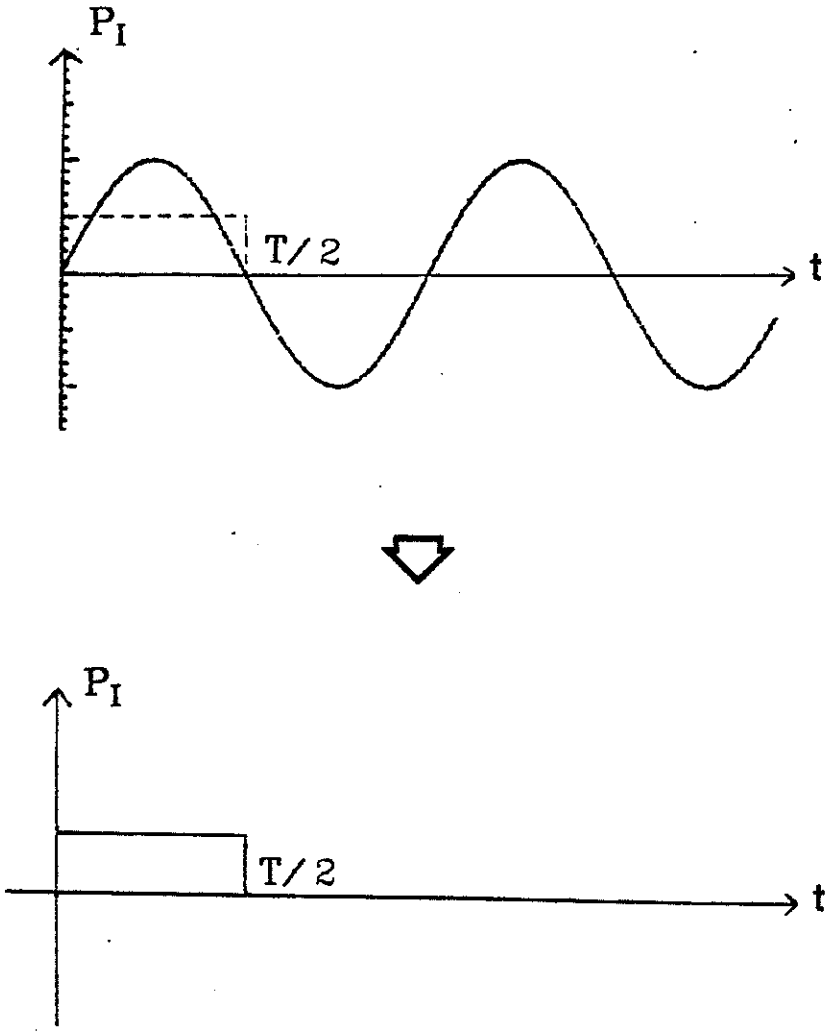

Figure 6: Pressure approximation at the fracture boundary.

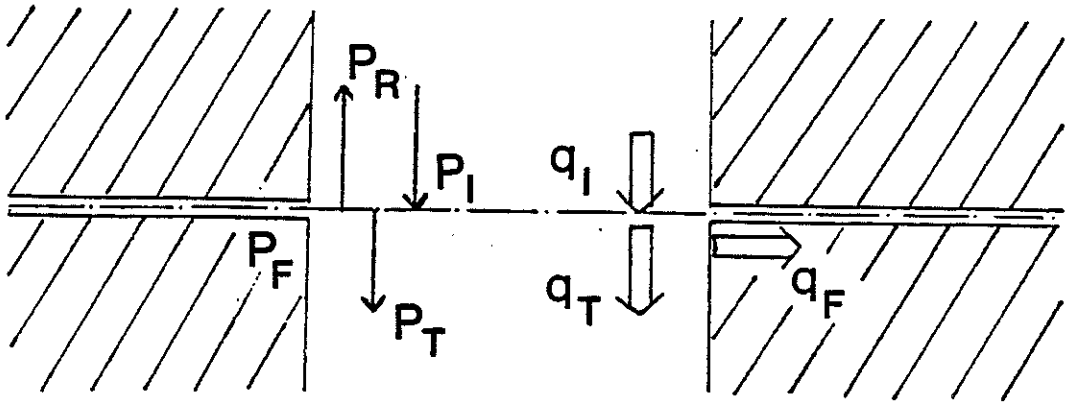

Figure 7a: Boundary conditions for the single fracture case.

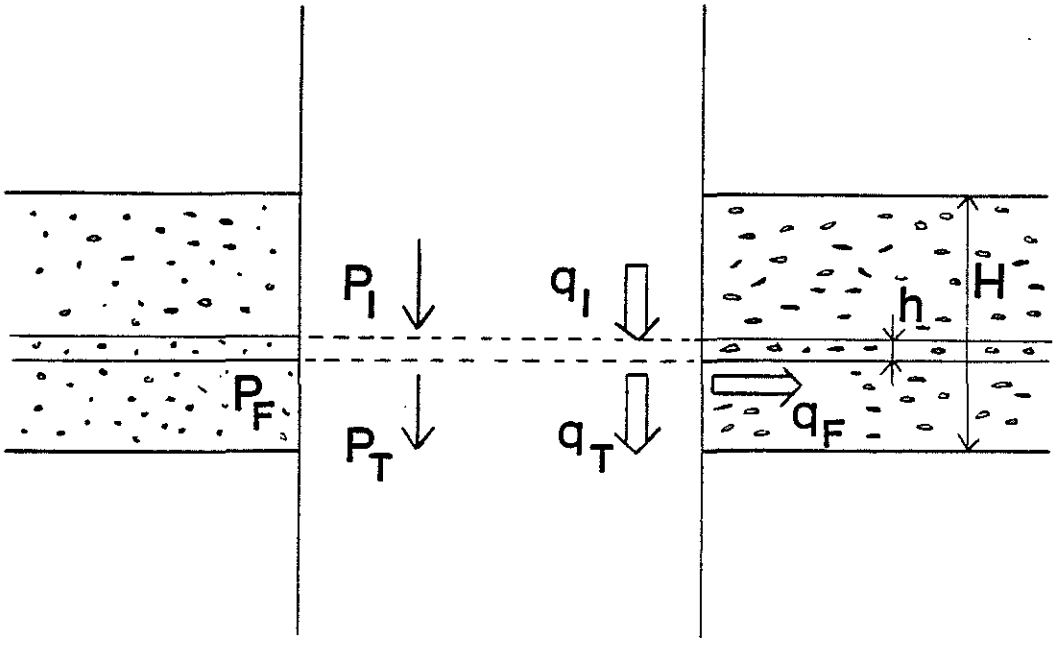

Figure 7b: Boundary conditions for the porous medium case.

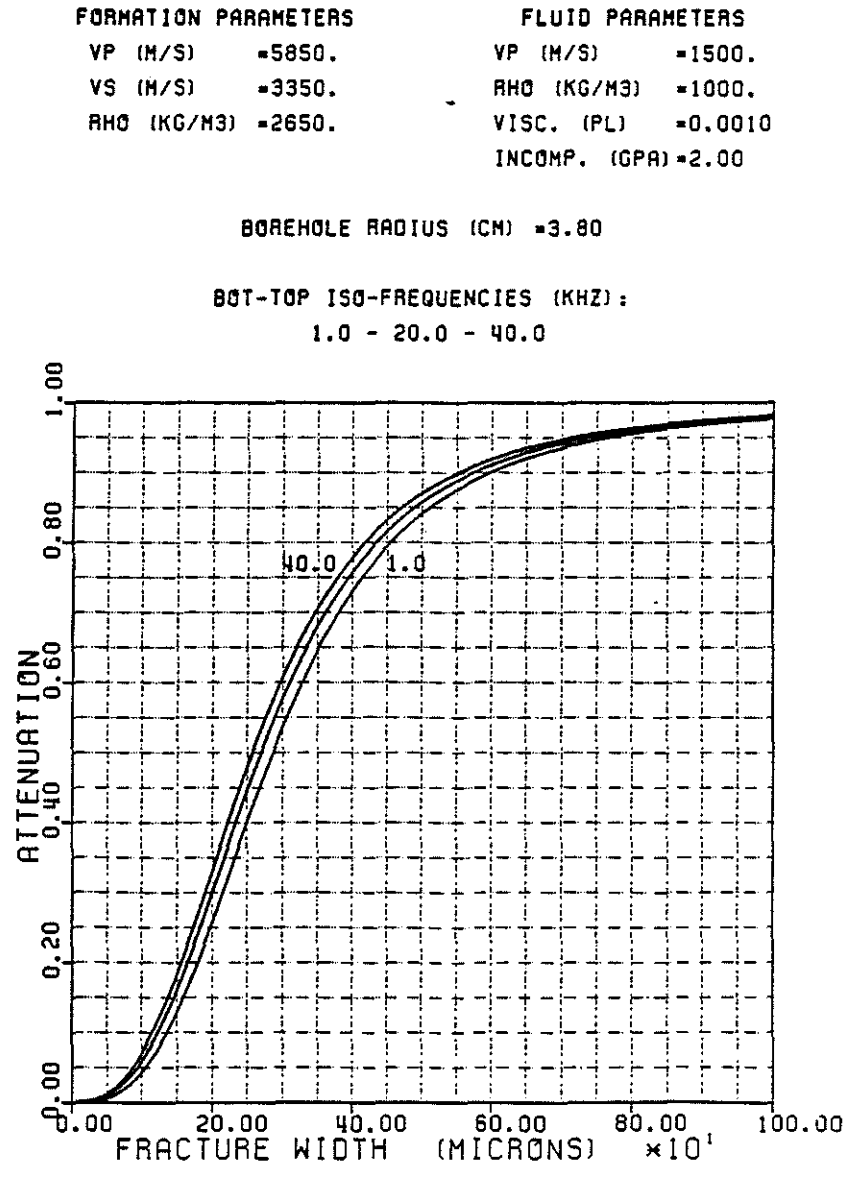

Figure 8: Frequency effect on attenuation - Case of a single fracture.

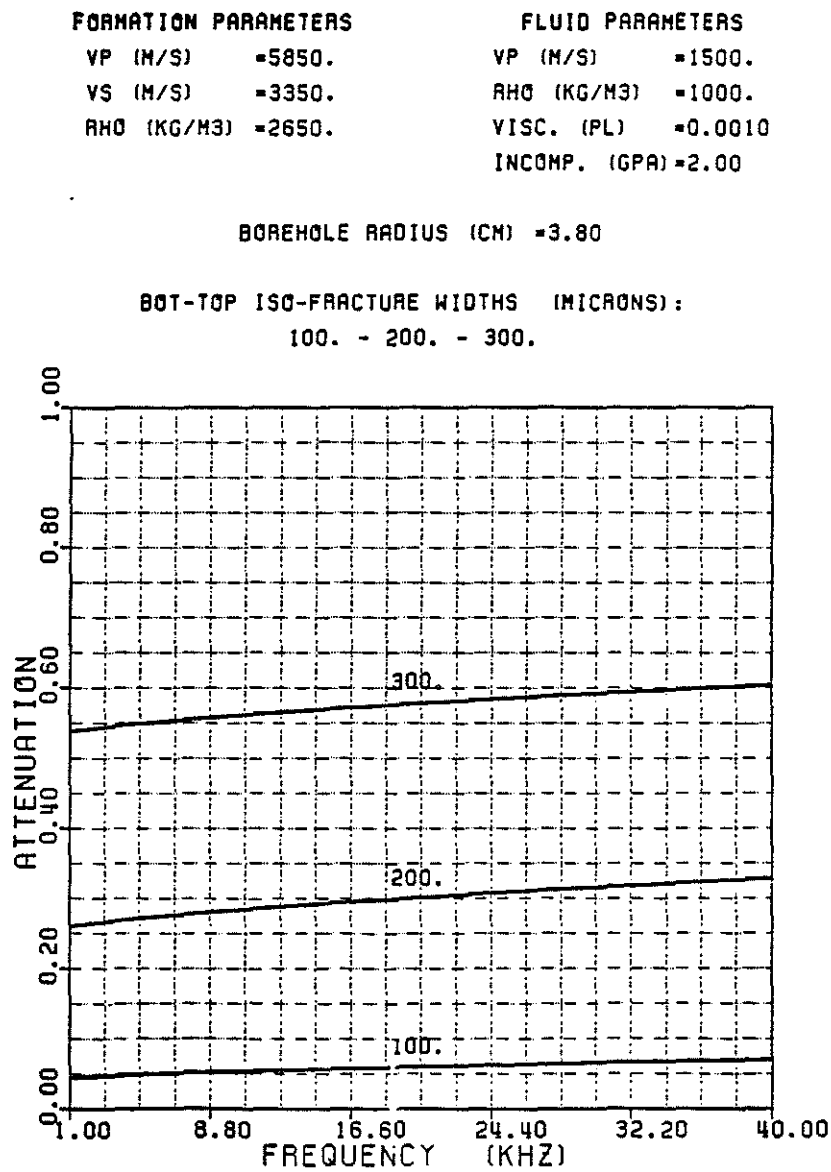

Figure 9: Attenuation versus frequency - Case of a single fracture.

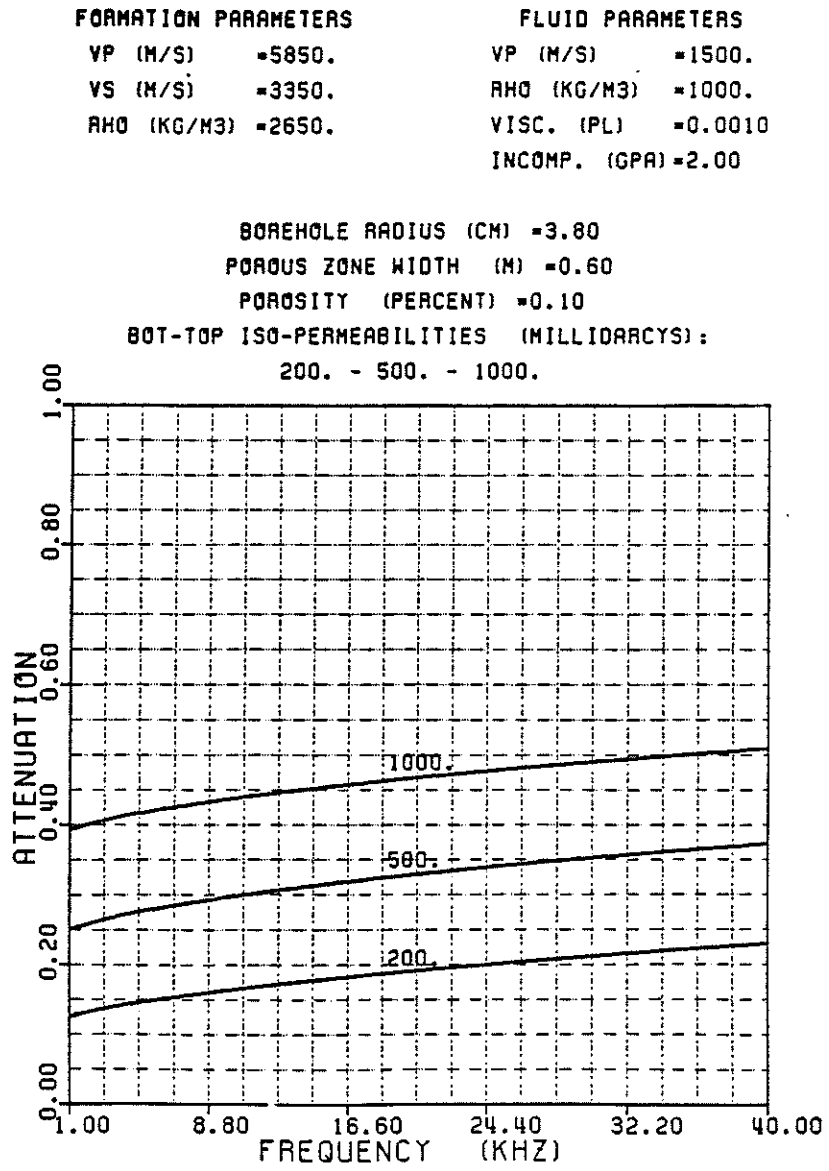

Figure 10: Attenuation versus frequency - Case of a porous medium.

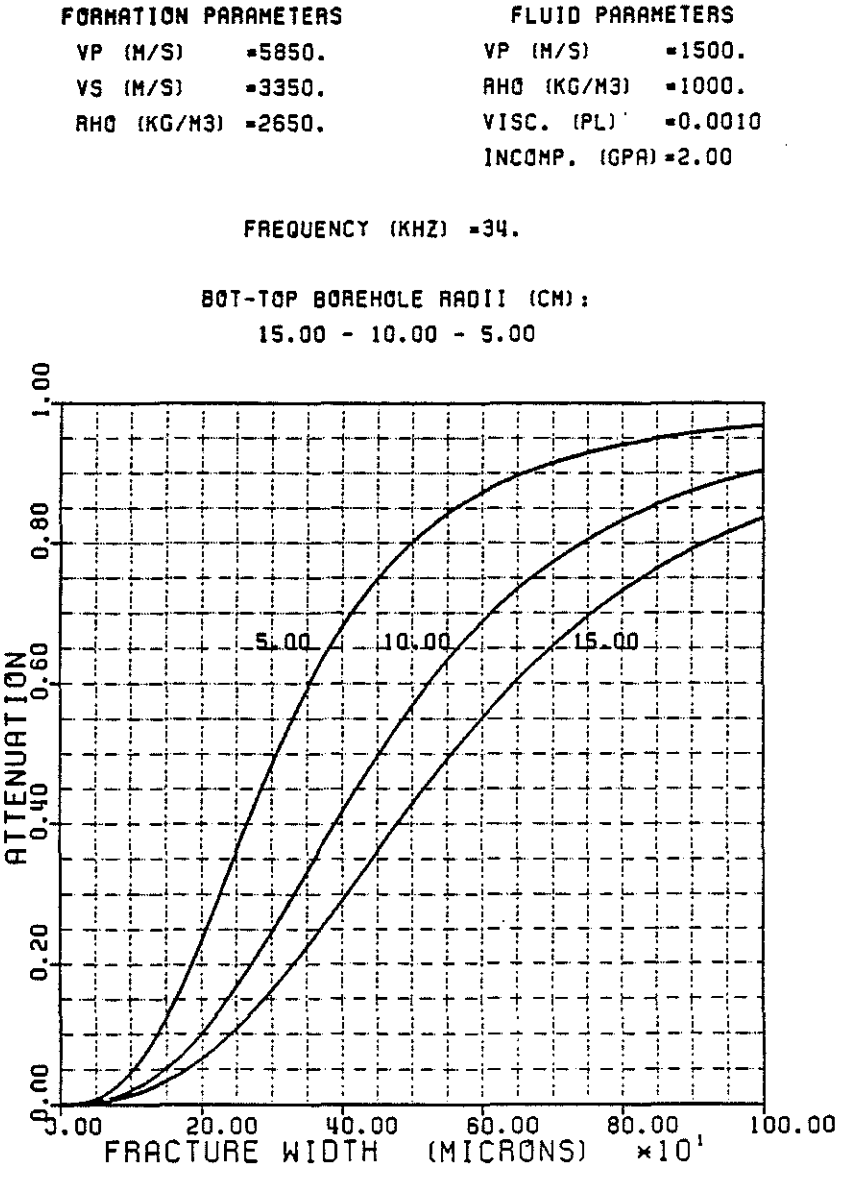

Figure 11: Borehole radius effect on attenuation - Case of a single fracture.

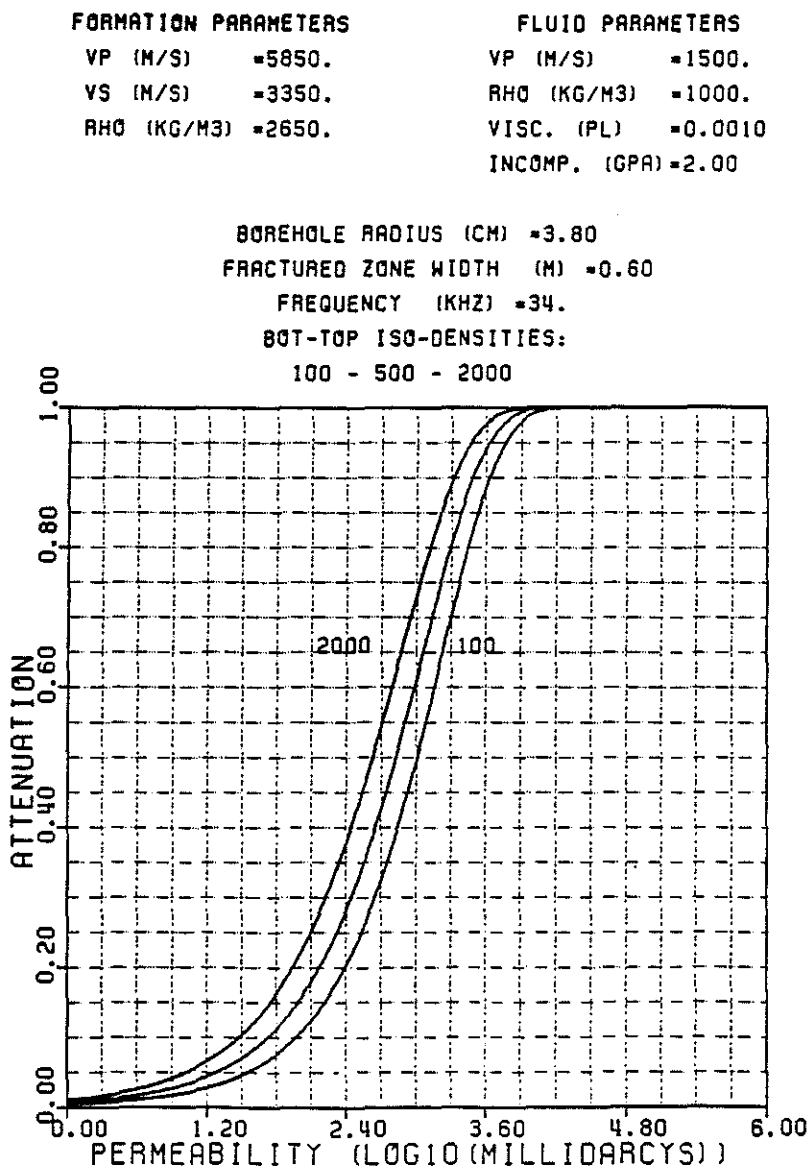

Figure 12: Attenuation versus permeability - Case of a fractured zone.

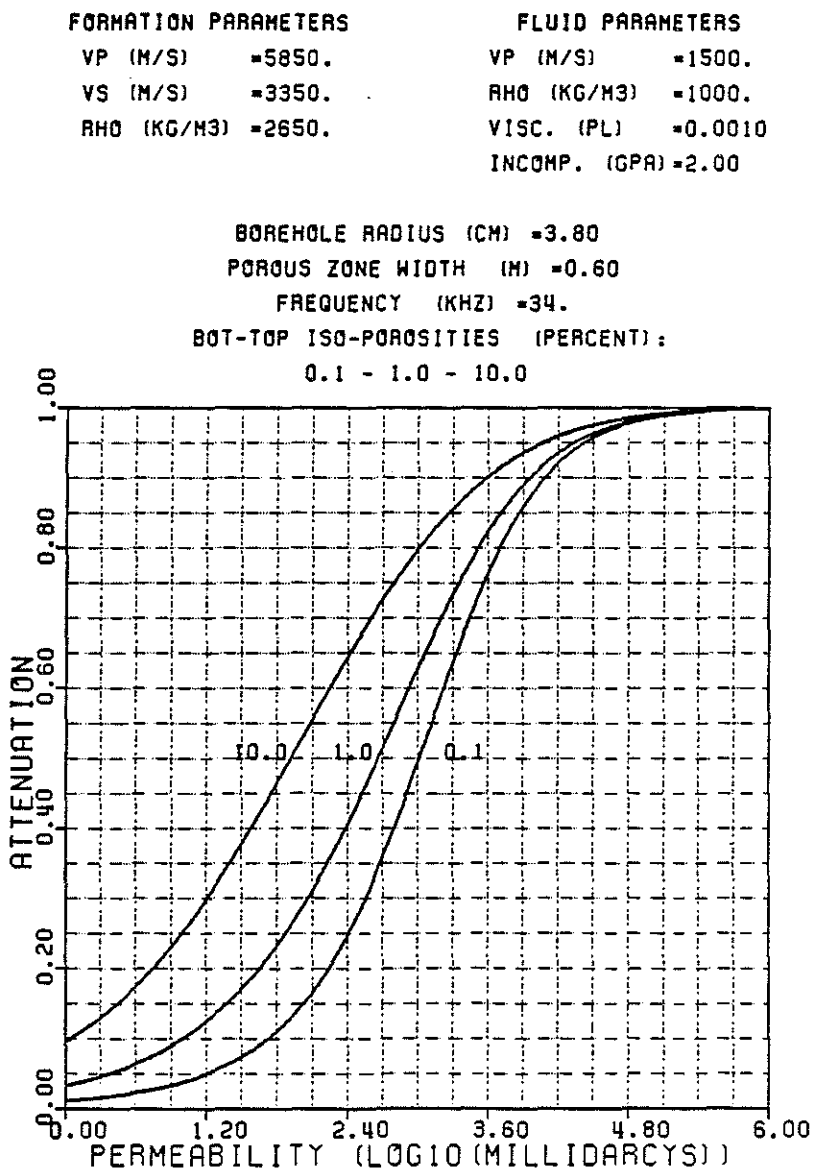

Figure 13: Attenuation versus permeability - Case of a porous zone.

FORMATION PARAMETERS		FLUID PARAMETERS	
VP (M/S)	=5850.	VP (M/S)	=1500.
VS (M/S)	=3350.	RHO (KG/M3)	=1000.
RHO (KG/M3)	=2650.	VISC. (PL)	=0.0010
		INCOMP. (GPA)	=2.00

BOREHOLE RADIUS (CM) =3.80

FREQUENCY (KHZ) =34.00

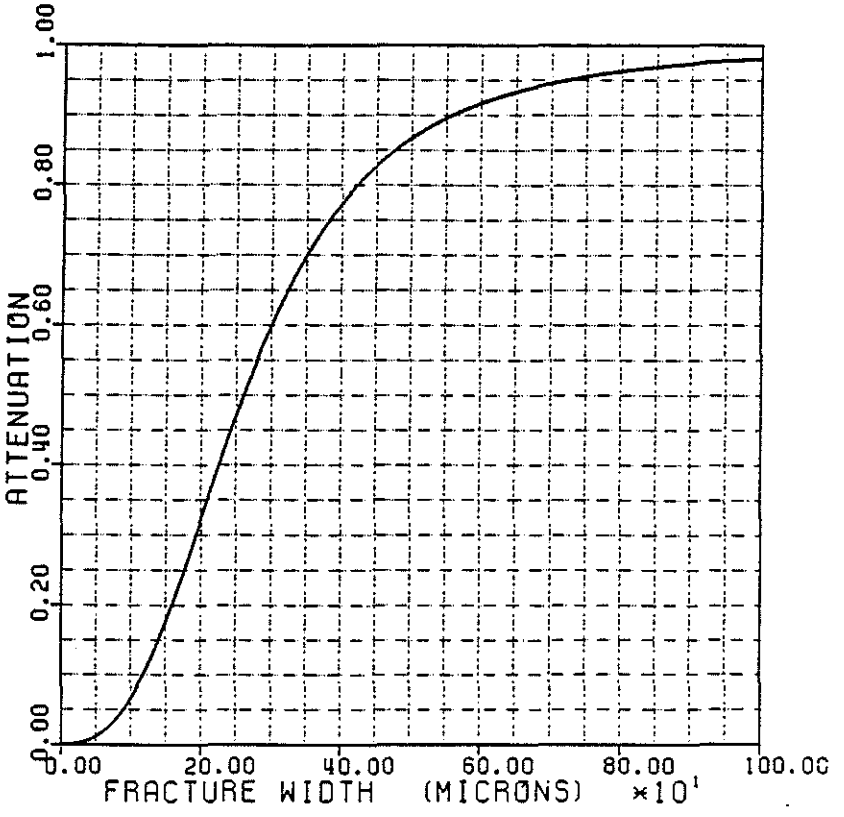

Figure 14: Fracture aperture estimation from observed attenuation.